Hydrogen Bonding and the Cryoprotective Properties of Glycerol/Water Mixtures

Jennifer L. Dashnau,* Nathaniel V. Nucci, Kim A. Sharp, and Jane M. Vanderkooi

Johnson Research Foundation, Department of Biochemistry and Biophysics, School of Medicine, University of Pennsylvania, Philadelphia, Pennsylvania 19104

Received: March 26, 2006; In Final Form: May 11, 2006

Molecular dynamics simulations and infrared spectroscopy were used to determine the hydrogen bond patterns of glycerol and its mixtures with water. The ability of glycerol/water mixtures to inhibit ice crystallization is linked to the concentration of glycerol and the hydrogen bonding patterns formed by these solutions. At low glycerol concentrations, sufficient amounts of bulk-like water exist, and at low temperature, these solutions demonstrate crystallization. As the glycerol concentration is increased, the bulk-like water pool is eventually depleted. Water in the first hydration shell becomes concentrated around the polar groups of glycerol, and the alkyl groups of glycerol self-associate. Glycerol−glycerol hydrogen bonds become the dominant interaction in the first hydration shell, and the percolation nature of the water network is disturbed. At glycerol concentrations beyond this point, glycerol/water mixtures remain glassy at low temperatures and the glycerol−water hydrogen bond favors a more linear arrangement. High glycerol concentration mixtures mimic the strong hydrogen bonding pattern seen in ice, yet crystallization does not occur. Hydrogen bond patterns are discussed in terms of hydrogen bond angle distributions and average hydrogen bond number. Shift in infrared frequency of related stretch and bend modes is also reviewed.

I. Introduction

Glycerol, a trihydric alcohol, is used by a number of organisms for its cryoprotective properties.[1−4] In nature, glycerol is used in high concentrations as a colligative cryoprotectant that raises the osmolality of body fluids and reduces the water available to form extracellular ice.[5] Glycerol is also active in maintaining the structure of biological macromolecules and in promoting protein self-assembly through preferential hydration.[6,7] Experimentally, the glass-forming properties of high glycerol/water mixtures have made these solutions an attractive solvent system for low-temperature studies of proteins.

To understand how glycerol functions as a cryoprotectant, the physical properties of glycerol and its mixtures with water have been studied extensively by a number of methods including molecular dynamics;[8,9] thermodynamic measurements;[10−12] and broadband dielectric,[13,14] NMR,[15−17] infrared (IR),[18,19] and Raman[20] spectroscopy. While these studies have provided useful insights for understanding the general behavior of glycerol/water mixtures, the manner in which glycerol affects the organization and H-bonding of water is yet to be elucidated.

In this work, the H-bond patterns of glycerol/water mixtures were examined through both theoretical and experimental approaches. Analysis of molecular dynamics (MD) simulations of various glycerol/water mixtures was performed using the technique developed by Sharp et al.[21−25] This technique was used to determine the influence of solute molecules on the distribution of H-bond angle geometries in the surrounding water structure. Additionally, Fourier transform infrared spectroscopy (FTIR) was used to identify how H-bonding of certain groups was influenced by the concentration of glycerol in solution. We discuss the results in terms of how the H-bond patterns present in glycerol/water mixtures affect the cryoprotective properties of these solutions.

* To whom correspondence should be addressed. E-mail: jdashnau@mail.med.upenn.edu.

II. Materials and Methods

A. Materials. Glycerol (99.5%), glycerol-d_3 (98 atom % D), glycerol-d_8 (98 atom % D), and D_2O (99.8 atom % D) were supplied by Sigma (St. Louis, MO). Water was deionized and distilled prior to use.

B. Infrared Spectra and Analysis. For examination of the CH stretch modes and HOH bend modes, samples were prepared by weight using glycerol-d_3/D_2O and glycerol/H_2O, respectively, to obtain molar fractions of glycerol, x_{glyc}, from 0.1 to 1.0 in 0.1 increments. To examine the OH stretch modes, samples were prepared by volume at room temperature as follows (D_2O/H_2O/glycerol-d_8/glycerol): water (95:5:0:0); 20:80 glycerol/water (G/W) (75:5:20:0); 40:60 G/W (55:5:40:0); 60:40 G/W (35:5:60:0); 80:20 G/W (15:5:80:0); and glycerol (0:0:95:5). Table 1 lists the glycerol/water mixtures tested.

Samples were placed between two 1-mm CaF_2 windows, and infrared spectra were obtained with a Bruker IFS 66 Fourier transform IR spectrophotometer (Bruker, Brookline, MA). The sample compartment was purged with nitrogen to reduce the contribution from water vapor. The signal was monitored using an HgCdTe (MCT) detector. All spectra were taken in transmission mode with a spectral resolution of 2 cm^{-1}. Spectra were processed with atmospheric correction, Savitsky−Golay smoothing, baseline correction, and conversion to absorbance in OPUS v.5.0 (Bruker) prior to peak fitting.

For the temperature-dependent OH stretch mode, spectra were taken at 5 or 10 K intervals from 295 K to 10, 20, or 30 K with temperature modulated by an ADP closed cycle Helitran cryostat (Advanced Research Systems, Allentown, PA) and a Scientific Instruments model 9650 temperature controller (Scientific Instruments, West Palm Beach, FL). Samples were sealed between CaF_2 windows with no spacer. Sample thickness was measured interferometrically to be ~9 μm.

PeakFit v.4.11 (SYSTAT, Point Richmond, CA) was used to analyze the CH stretch and HOH bend modes of glycerol.

10.1021/jp0618680 CCC: $33.50
Published on Web 06/21/2006

TABLE 1: Glycerol/Water Composition of Mixtures Tested for Temperature-Dependent IR Measurements[a]

v/v	w/w	x_{glyc}	% O−H	final % H
20/80	24/76	0.06	9/91	6
40/60	46/54	0.14	20/80	7
60/40	65/35	0.27	36/64	8
80/20	84/16	0.50	60/40	10

[a] Columns include for each glycerol−water mixture: (1) volume ratio, (2) weight ratio, (3) glycerol molar fraction, (4) number ratio of hydroxyl groups, and (5) the total H content in solution.

For the CH stretch, peaks in the 2800−3050 cm^{-1} region were fit to Voigt functions and a linear, two point baseline. Peak position as a function of glycerol concentration was fit to an exponential decay curve in SigmaPlot 2001 v.9 (SPSS, Chicago, IL). For the HOH bend, peaks were fit in the region 1575−1725 cm^{-1} with a Voigt function. Peak position and full width at half-maximum were plotted in SigmaPlot.

C. Molecular Dynamics Simulations. All simulations were performed with the molecular dynamics program CHARMM v.27b2[26] using the all-atom CHARMM22 force field for glycerol[27] and the TIP3P water model.[28] For each simulation, glycerol/water solvent boxes were prepared by adding glycerol molecules (αα-isomer[9]) at random positions with random orientations to an equilibrated water box of side length 18.856 Å provided by CHARMM. The number of glycerol molecules added was dependent upon the desired concentration of glycerol for each simulation. Water molecules overlapping glycerol within 1.7 Å were deleted. Additional water molecules were randomly removed to approximate the desired glycerol/water ratio. The solvent boxes were then minimized with a series of adopted-basis Newton−Raphson (ABNR) minimizations with no constraints. After minimization, the boxes were equilibrated under the CVT ensemble for 1 ns, followed by the CPT ensemble for 1 ns.

The pre-equilibrated glycerol/water boxes were joined to construct larger cubic solvent boxes with side lengths of 56−59 Å. Again, water molecules were randomly removed to adjust the glycerol/water ratio to the final desired concentration. Side-lengths for each glycerol/water box were calculated and set so the density would correspond to experimental values.[29] The system was then equilibrated for a total of 250 ps followed by production dynamics simulations run for a total of 500 ps. Equilibration and dynamics were performed using the Verlet integrator in steps of 1 fs at constant temperature of 300 K and constant volume. Chemical bonds involving hydrogen atoms were constrained using the SHAKE algorithm.[30] A nonbond cutoff of 12 Å was used, and nonbond interactions were decreased to zero between distances of 10 and 11 Å by applying a switching function. Additionally, cubic periodic boundary conditions with the minimum image convention were employed to replicate water atoms to prevent artifacts introduced from a solvent boundary.

D. H-Bond Angle Distribution Analysis. Following production of the 500 ps trajectory, PRAM,[31] a program developed by the Sharp group, was used to analyze H-bonding. Solute atoms were first classified according to partial charge: atoms were designated nonpolar if their partial charge magnitude was less than 0.35 and polar if it was greater than or equal to 0.35. Water molecules were then classified as first shell if they were within the first hydration shell of any solute atom type, i.e., within 5.6 or 3.4 Å of a C or O atom, respectively. Water molecules not within the first hydration shell were classified as bulk water. H-bond angles (θ) are defined as the angle formed by H−O···O. The distribution of water−water H-bond angles between pairs of water molecules in the first hydration shell or between pairs of bulk water molecules separated by less than 4 Å was then calculated for each saved frame of the trajectory. The H-bond angle probability distributions, $P(\theta)$, were separately accumulated according to the type of solute atoms inducing the structure. For example, for a water pair, if one of the water oxygen atoms was closest to a nonpolar solute atom and the other was closest to a polar solute atom, the H-bond angle was classified as part of the nonpolar−polar (*np*) distribution. The other three possible classes, nonpolar−nonpolar (*nn*), polar−polar (*pp*), and bulk−bulk (*bulk*) distributions were also calculated.

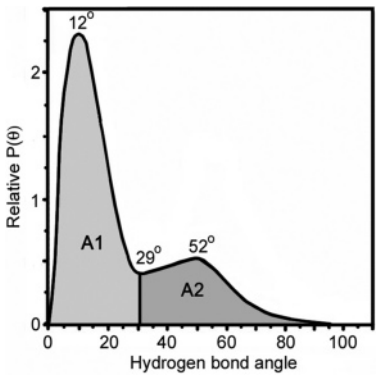

Figure 1. Typical $P(\theta)$ distribution. The low-angle and high-angle peaks are centered around 12° and 52°, respectively. The saddle point at 29° is used as a boundary in integration of the areas of these two peaks, A1 and A2.

The functionality of PRAM was extended from previous versions to also calculate $P(\theta)$ between the OH groups of additional molecules, in this case, glycerol. Three new distributions were added: glycerol−water (*gw*), glycerol−glycerol intramolecular (*ggi*), and glycerol−glycerol intermolecular (*gg*). In these cases, the $P(\theta)$ between glycerol OH groups or between glycerol OH groups and water separated by less than 4 Å were calculated and saved according to interaction type.

For $P(\theta)$ exhibiting a typical bimodal distribution (see Figure 1), the areas beneath the peaks A1 (low angle, centered at 12°) and A2 (high angle, centered at 52°) were integrated in Origin v.6 (OriginLab, Northampton, MA). The saddle point at 29° was used as a boundary for the integration. The ratio of these areas, A1/A2, was then used to compare H-bonding across different glycerol/water conditions.

E. Glycerol Conformer Determination. The structure of a glycerol molecule can be classified according to its backbone conformation. Each glycerol can be assigned two torsion angles formed by the three carbon atoms and two terminal oxygen atoms. The terminal CH_2OH group can rotate about the C−C bond, yielding α, β, and γ conformations.[32] In our simulations, the cis conformation was set to 0°, and rotation of the OH group relative to CH_2OH was assigned to positive (clockwise) and negative (counterclockwise) values between 0° and 180°. Therefore, α, β, and γ conformations correspond to the following torsion angle (ϕ) ranges: α, ($120° \le \phi \le 180°$) or ($-180° \le \phi \le -120°$); β, ($-120° < \phi \le 0°$); and γ, ($0° < \phi < 120°$). Figure 2 illustrates the position of the OH group relative to CH_2OH for each conformation. Since there are two such torsion angles in glycerol, a total of six backbone conformers are possible: αα, αβ, αγ, $\beta\beta$, $\beta\gamma$, and $\gamma\gamma$. For each saved frame of the molecular dynamics trajectory, the distribution of glycerol backbone conformations was calculated and compared across glycerol concentration.

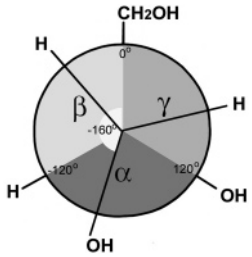

Figure 2. Definition of glycerol backbone conformers. The OH group is rotated about the C−C bond. The cis conformation is set to 0°, and rotations of the OH group relative to CH_2OH are assigned to positive (clockwise) and negative (counterclockwise) values between 0° and 180°. Backbone conformers are classified as follows: α, ($120° \leq \phi \leq 180°$) or ($-180° \leq \phi \leq -120°$); *β*, ($-120° < \phi \leq 0°$), and *γ*, ($0° < \phi < 120°$). An α-conformer with a torsion angle of −160° is shown as an example.

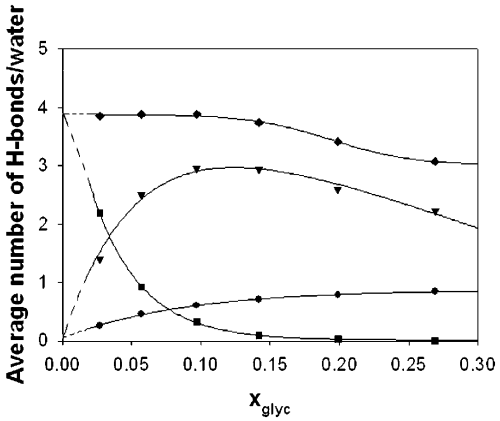

Figure 3. Average number of H-bonds per water as a function of x_{glyc}. Symbols represent the total average number of H-bonds per water (diamonds) as well as contributions from subsets of H-bonds: *bulk* (squares), solvation shell consisting of *nn*, *pp*, and *np* (triangles), and *gw* (circles).

III. Results and Discussion

A. Bulk Water Depletion. The average H-bonding characteristic of water and glycerol molecules as a function of glycerol concentration is important for understanding how glycerol functions as a colligative solute. Figure 3 shows the average number of H-bonds/water as calculated from molecular dynamics simulations. The average number of H-bonds/water is relatively constant at 3.9 H-bonds in the region $0 < x_{glyc} < 0.15$. However, examination of the contributions of H-bond subsets to this total reveals that the characteristics of water in this region are in fact changing. As x_{glyc} is increased through $x_{glyc}(0.15)$, the average number of H-bonds made in *bulk* decreases rapidly from 2.2 H-bonds/water at $x_{glyc}(0.03)$ to nearly zero H-bonds/water at $x_{glyc}(0.15)$. Concurrently, the number of H-bonds made to waters in the first hydration shell (including *nn*, *np*, and *pp* interactions) increases in an almost opposite fashion. The contribution of first hydration shell H-bonds to the average number of H-bonds/water increases from 1.4 at $x_{glyc}(0.03)$ to 2.9 at $x_{glyc}(0.15)$. Additionally, the number of H-bonds/water contributed by *gw* interactions increases from 0.3 at $x_{glyc}(0.03)$ to 0.7 at $x_{glyc}(0.15)$.

The H-bonding behavior of water in this region can be explained by considering the effect of increasing glycerol concentration. The increase in x_{glyc} requires that some of the bulk water molecules be employed in solvation of glycerol molecules through the first hydration shell. As a result, the population of water molecules in the first hydration shell grows at the expense of the bulk water pool. The population of water molecules H-bonded to glycerol OH groups also increases as a result.

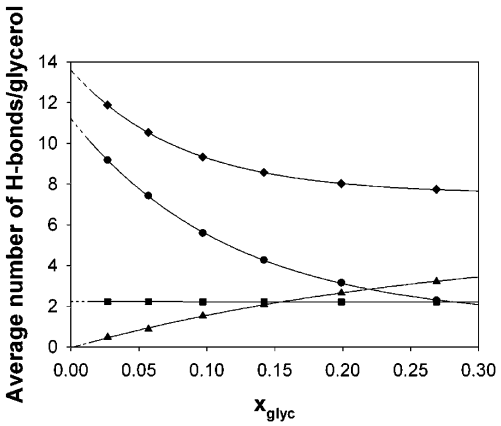

Figure 4. Average number of H-bonds per glycerol as a function of x_{glyc}. Symbols represent the total average number of H-bonds per glycerol (diamonds) as well as contributions from subsets of H-bonds: *gw* (circles), *ggi* (squares), and *gg* (triangles).

The experimental data of Parsons et al.[11] and To et al.[12] support the results of our molecular dynamics simulations. They found that in the region $x_{glyc} < 0.15$, the H-bond probability of bulk water away from solutes is gradually reduced, yet the basic features of liquid water are retained. At $x_{glyc} > 0.15$, the percolation nature of the H-bond network becomes greatly reduced as do the characteristics of bulk-like water. Our simulations reflect the reduction of bulk-like water characteristics above this glycerol concentration.

Beyond $x_{glyc}(0.15)$, the total number of H-bonds/water begins to decrease. At $x_{glyc} > 0.15$, there is no longer a bulk water pool from which to transfer water molecules to the first hydration shell of additional glycerol molecules. As a result, the first hydration shell waters are no longer sufficient to fully solvate the glycerol molecules; this idea is supported by the decrease in first hydration shell H-bonds/water in this region. At $x_{glyc}(0.27)$, a concentration known to prevent ice formation, the average number of first hydration shell H-bonds/water is 2.2. This value is in the range of the two-dimensional percolation threshold of hydration water: 2.0−2.3 hydration shell H-bonds/water.[33] The percolation threshold defines the point above which there are a sufficient number of water molecules to create a spanning network of water. (Although the number of hydration shell H-bonds/water at $x_{glyc} < 0.05$ is below the percolation threshold of hydration water, bulk water is present beyond the first hydration shell and has the effect of introducing three-dimensionality to the network.[33])

To solvate the increasing glycerol population, a new mechanism must be used. Figure 4 illustrates the total average number of H-bonds/glycerol as calculated from molecular dynamics simulations. The total number of H-bonds/glycerol decreases exponentially from 11.8 at $x_{glyc}(0.03)$ to 8.5 at $x_{glyc}(0.15)$. The decrease of H-bonds/glycerol in the lower x_{glyc} region is the result of a decreasing contribution from *gw* interactions. However, at approximately $x_{glyc}(0.22)$, the contribution from *gg* interactions begins to negate the decrease from *gw* interactions, causing the number of H-bonds/glycerol to become steady at about 7.5. This value is similar to that calculated by Sarkar and Joader, 6.5 OH neighbors, that was obtained from X-ray diffraction data with a smaller cutoff distance of 2.95 Å.[34] Our cutoff, 4 Å, is larger and thus yields a slightly higher value of the average H-bonds/glycerol. H-bonding between glycerol

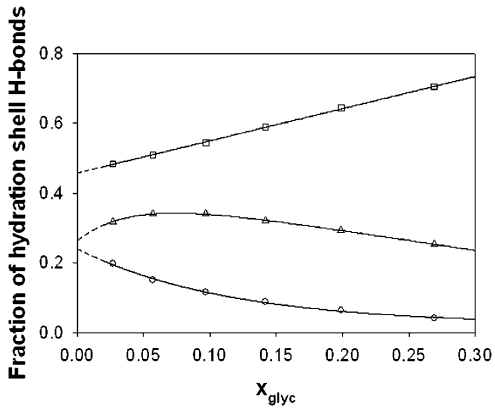

Figure 5. Fraction of first hydration shell H-bonds due to *nn* (open circles), *np* (open triangles), and *pp* (open squares) groups as a function of x_{glyc}.

molecules compensates for the lack of additional water molecules needed to solvate glycerol at higher x_{glyc}.

Interestingly, the average number of H-bonds/glycerol from *ggi* interactions does not change within the conditions simulated. Since the conformational arrangement of glycerol OH groups may affect H-bonding patterns, the distribution of glycerol backbone conformations was calculated to confirm that the mixtures maintained experimentally relevant distributions. Across all concentrations studied, the conformer distribution after equilibration from an all $\alpha\alpha$ starting configuration was approximately equal: $\alpha\alpha$, 40%; $\alpha\gamma$, 30%; $\alpha\beta$, 20%; $\gamma\gamma$ and $\beta\gamma$, 5%; and $\beta\beta$, 0%. These values show some similarity to those previously found for simulation of pure glycerol: $\alpha\alpha$, 48%; $\alpha\gamma$, 46%; $\alpha\beta$, 1.4%; $\gamma\gamma$, 4%; $\beta\gamma$, 0.2%; and $\beta\beta$, 0%.[9] The largest differences appear in the $\alpha\beta$ and $\beta\gamma$ populations which are both increased at the expense of the $\alpha\gamma$ population. The values are also similar to experimental values from NMR data.[8] Here, populations for liquid phase pure glycerol are cited as approximately the following: $\alpha\alpha$, 20%; $\alpha\gamma$, 30%; $\alpha\beta$, 20%; $\gamma\gamma$, 10; $\beta\gamma$, 15%; and $\beta\beta$, 5%. The largest difference in this case is that our simulations show a larger $\alpha\alpha$ population with slightly smaller $\gamma\gamma$, $\beta\gamma$, and $\beta\beta$ populations. It should be noted, however, that the differences may be the result of the presence of water molecules in our simulations. Conformation distribution values for glycerol/water mixtures were not found in existing literature.

B. Alkyl Backbone Interactions. In addition to the depletion of bulk water molecules in higher x_{glyc} mixtures, the alkyl backbone of glycerol also becomes less associated with surrounding first hydration shell water molecules. Figure 5 shows the fraction of first hydration shell water molecules associated with the classes of glycerol−water interactions as a function of x_{glyc}. As x_{glyc} is increased, the fraction of first hydration shell waters surrounding *pp* groups, i.e., the glycerol OH groups, becomes a larger portion of the total water molecules in this shell; *pp* increases from 0.48 at $x_{glyc}(0.03)$ to 0.70 at $x_{glyc}(0.27)$. Meanwhile, the fraction surrounding *nn* groups, or glycerol CH groups, decreases from 0.20 at $x_{glyc}(0.03)$ to 0.04 at $x_{glyc}(0.27)$. The *np* population, which signifies water pairs surrounding a CH and an OH group, shows mixed behavior, but on a whole decreases slightly as well. The increase of the *pp* population with decrease of the *nn* population suggests that as x_{glyc} increases, water molecules in the first hydration shell are more likely to be found around glycerol OH groups than CH groups. This result implies that the CH groups are surrounded by something other than water: glycerol. Alkyl backbone clustering, a possible explanation for this result, was previously proposed to be present in high glycerol concentration glycerol/water mixtures.[11]

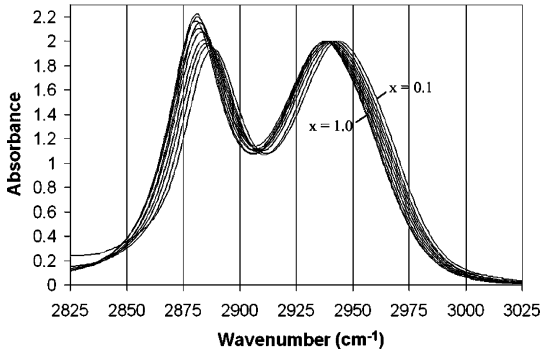

Figure 6. Infrared spectra of the CH stretch region of glycerol/water mixtures with x_{glyc} ranging from 0 to 1 in 0.1 increments. Spectra were normalized in the region of the higher frequency, antisymmetric stretch.

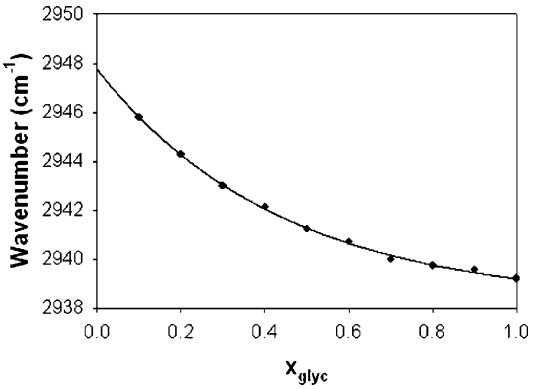

Figure 7. Peak frequency of the CH antisymmetric stretch mode as a function of $x_{glyc.}$

Infrared spectra of the CH stretch modes of glycerol at various x_{glyc} values were taken to further probe the behavior of these groups. Figure 6 shows the IR spectra in the CH stretch region as a function of x_{glyc}. Figure 7 illustrates the shift of peak frequency for the CH asymmetric stretch mode as a function of x_{glyc}. The frequency shifts from 2948 cm^{-1} at $x_{glyc}(0)$ to 2939 cm^{-1} at $x_{glyc}(1)$. The CH symmetric stretch mode (not shown) exhibits a similar shift.

Shifting of the CH stretch modes can be attributed to weak H-bonding between the glycerol CH groups and water or other glycerol OH groups. Previously, our group has shown that the CH groups of glycerol do not exhibit temperature-dependence, a result generally indicative of the lack of H-bonding.[19] However, the lack of temperature dependence of the CH stretch modes can be attributed to the insensitivity of the C−H···O bonds to angular deformations.[35] O−H···O bonds, which are more sensitive to geometrical fluctuations, exhibit a large temperature dependence in OH stretch frequency with temperature.[19] Gu, Kar, and Scheiner have shown that C−H···O H-bonds do exist and that H-bonding to an sp^3-hybridized CH group can induce a blue-shift in IR frequency of CH stretch modes.[35,36] Additionally, the frequency shift is sensitive to the acceptor group with which it is H-bonded; the CH asymmetric stretch of H_3CH shifts 10 cm^{-1} when H-bonded to OH_2 but only 5 cm^{-1} when bonded to CH_3OH.[35]

The CH groups of glycerol are more likely to be solvated by water at low x_{glyc} concentrations. As a result, water is available to interact with the CH groups in weak C−H···O H-bonds. The magnitude and direction of the frequency shift associated with the C−H···O interaction at low x_{glyc} relative to $x_{glyc}(1)$ is near +8.5 cm^{-1}, very similar to the change in frequency associated

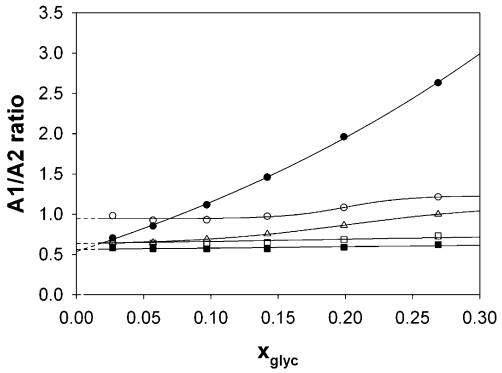

Figure 8. A1/A2 ratios of *bulk* (squares), *gw* (circles), *nn* (open circles), *np* (open triangles), and *pp* (open squares) as a function of x_{glyc}.

with forming an $H_3CH\cdots OH_2$ interaction listed above.[35] As x_{glyc} increases, the frequency shift relative to $x_{glyc}(1)$ drops exponentially. This decrease is expected considering that a methylated acceptor decreases the CH stretch frequency of the C−H···O donor. As other glycerol OH groups replace water molecules in the first hydration shell, glycerol CH groups are presented with increasingly weaker H-bond acceptors. Beyond $x_{glyc}(0.6)$, the point at which glycerol−water interactions are at a maximum,[10] there is little change in the CH stretch frequency. Hydrophobic clustering of CH groups may explain the small shift in CH stretch frequency at $x_{glyc} > 0.6$. The CH stretch mode was used previously to demonstrate hydrophobic clustering of *tert*-butyl alcohol molecules.[37] Here, the progressive decrease in CH stretch frequency of *tert*-butyl alcohol was concluded to be a result of changing the environment surrounding the CH groups; i.e., these group were surrounded less by water and therefore were associated in hydrophobic clusters.

C. Glycerol−Water H-Bond Linearization. The following question remains: How do bulk water depletion and alkyl backbone interactions influence the structure of water in glycerol/water mixtures? An analysis of H-bond angle geometries was used to address this question. Figure 8 shows the A1/A2 ratios for a number of interactions as a function of x_{glyc}. For most of the subsets, there is little change over the x_{glyc} range simulated. For example, the ratios for the *bulk* and *pp* distributions remain constant at 0.56 and 0.63, respectively. The constant A1/A2 ratio of the *bulk* distribution across all glycerol concentrations simulated attests to the idea that *bulk* water is relatively unaffected by solute and retains the characteristics of pure water. Indeed, the A1/A2 ratio of the *bulk* population is similar to the value expected for pure water, 0.75.[38]

Most notable, however, is the change in A1/A2 ratio for the *gw* distribution. As x_{glyc} approaches infinite dilution, the value for *gw* approaches that of the *bulk* and *pp* distributions. As x_{glyc} increases, the lower angle distribution, A1, grows greatly with respect to the higher angle distribution, A2. By $x_{glyc}(0.27)$, the A1 distribution is 2.5 times larger than the A2 distribution, indicating that H-bonds between glycerol and water are more linearly arranged.

The linearity of an H-bond, in the case of O−H···O bond, can be related to the H-bond stretch frequency exhibited by its

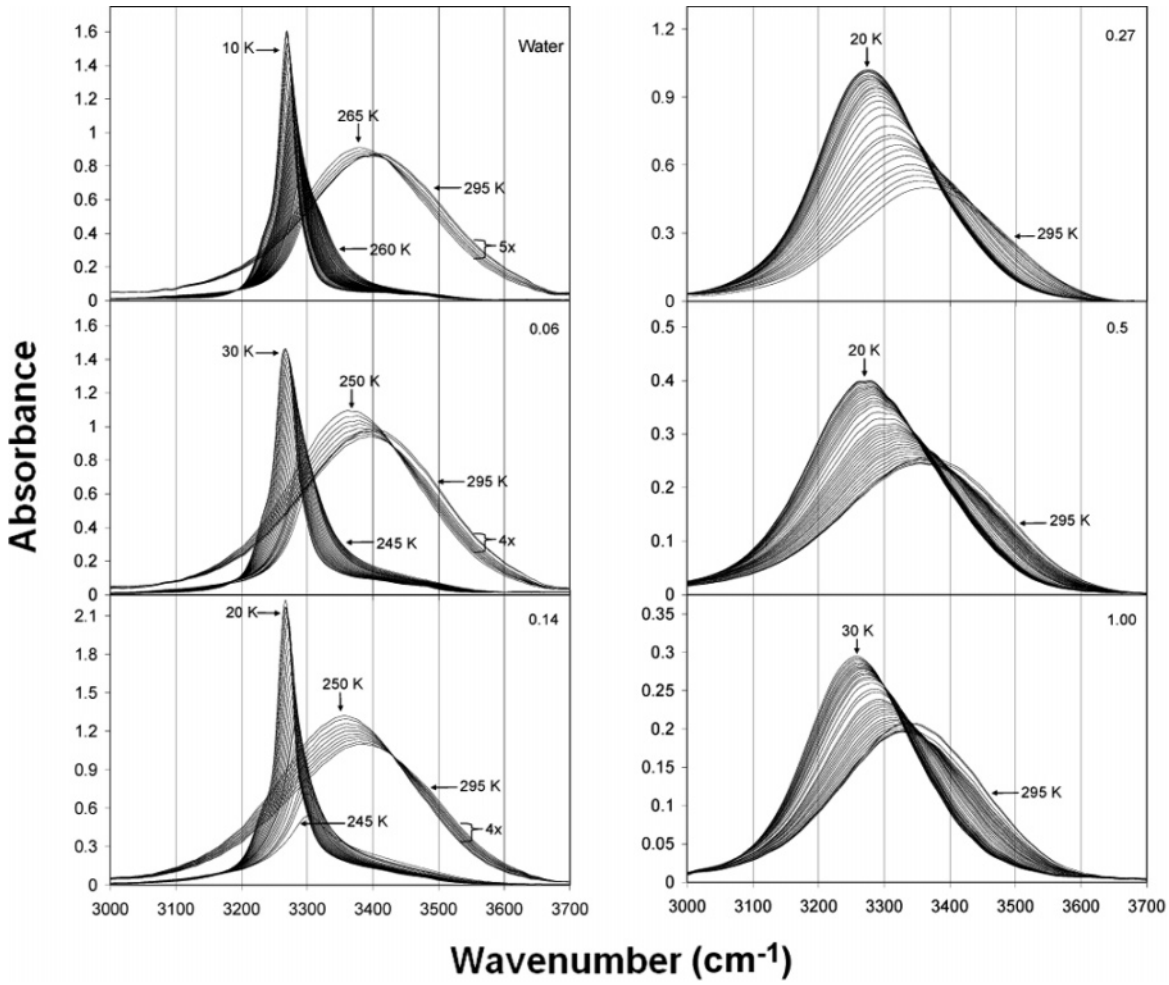

Figure 9. Infrared spectra of the OH stretch region of various glycerol/water mixtures from 295 K to 20 or 30 K. The x_{glyc} value appears in the top, right corner of each graph.

TABLE 2: OH Stretch Mode Peak Frequencies (cm^{-1}) of Glycerol/Water Mixtures at Room Temperature (295 K) and Low Temperature (20 or 30 K)

x_{glyc}	peak at 295 K	peak at 20/30 K
0.00	3403	3268
0.06	3396	3265
0.14	3380	3266
0.27	3361	3273
0.50	3363	3269
1.00	3337	3256

components; increased H-bonding shifts the OH stretch frequency to lower wavenumbers.[18] For example, ice exhibits a lower OH stretch frequency than water due to its strengthened H-bond interactions. This shift results from a weakening of the intramolecular OH force constant that is maximized when the H-bond acceptor and donor arranged linearly. Therefore, if the A1/A2 ratio of an H-bond interaction increases, implying a more linear distribution of H-bonds, it follows that IR spectra will show a decrease in frequency of the associated stretch modes.

Figure 9 shows the temperature-dependent IR spectra of various glycerol/water mixtures. At lower x_{glyc} values of 0, 0.06, and 0.14, the freezing of water is clearly visible by the appearance of sharp, lower frequency bands below 265 K (water) and 250 K (glycerol/water mixtures). As the temperature is lowered further, the ice band becomes increasingly narrow, the absorbance increases, and the band continues to shift. The higher x_{glyc} mixtures of 0.27, 0.50, and 1.00 do not show visible freezing. However, the OH stretch mode does narrow slightly, absorbance increases, and the band continues to shift.

Interestingly, at the lowest temperatures measured, the peak position of the OH stretch frequency for the higher x_{glyc} mixtures is almost identical to that of the lower x_{glyc} mixtures, despite the failure to form ice. Table 2 shows the OH stretch mode peak frequency at room temperature and at the lowest temperature measured for a number of glycerol/water mixtures. At room temperature, increasing x_{glyc} lowers the OH stretch mode peak frequency with respect to pure water; $x_{glyc}(0)$ and $x_{glyc}(1)$ have frequencies of 3403 and 3337 cm^{-1}, respectively. However, at the lowest temperatures measured (10−30 K), all mixtures tested exhibit peaks in the 3265−3273 cm^{-1} range with the exception of pure glycerol which had a slightly lower peak frequency of 3258 cm^{-1}. The similarity in low temperature OH stretch mode peak frequency indicates that although high concentration glycerol/water mixtures do not crystallize, the average OH H-bond in the glycerol/water mixtures is of the same energy (same geometry) as that found in ice.

The OH stretch region provides only general information on the H-bonding network as a whole since the individual contributions from the OH modes of glycerol and water cannot be separated. However, the HOH bend mode around 1650 cm^{-1} can be used to inspect the contribution from water since this band does not overlap with any modes of glycerol. Shifts in the HOH bend mode are inversely proportional to shifts in the OH stretch mode,[39] and a shift in the HOH bend mode frequency to higher wavenumber is generally indicative of increased H-bonding.[18] Figure 10 shows the IR spectra in the HOH bend region as a function of x_{glyc}. Figure 11 shows the shift in peak frequency as a function of x_{glyc}. The shift in peak frequency to higher wavenumber indicates that as x_{glyc} increases, water molecules are involved in more linear H-bonds. At the same time, Figure 12 shows that the HOH bend mode narrows as x_{glyc} is increased. This trend is consistent with a reduction of inhomogeneous broadening that results from a large distribution of H-bond angles and distances;[18] the environment surrounding

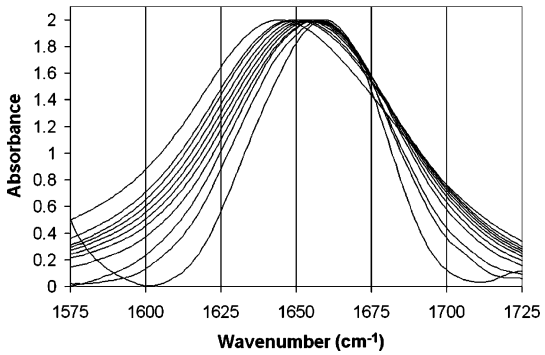

Figure 10. Normalized infrared spectra of the HOH bending region of various glycerol/water mixtures.

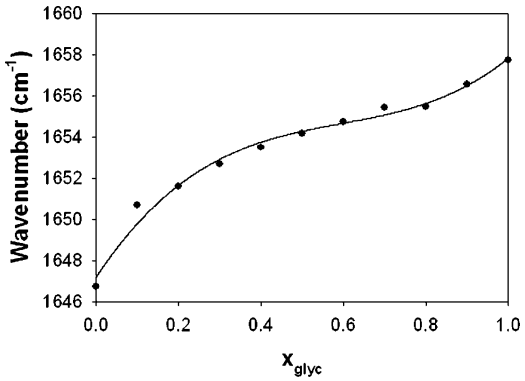

Figure 11. Peak frequency of the HOH bending mode as a function of x_{glyc}.

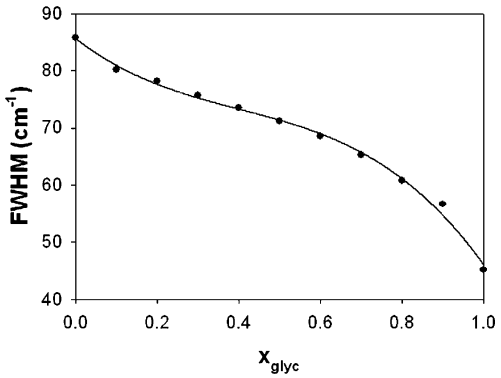

Figure 12. Full width at half-maximum of the HOH bending mode as a function of x_{glyc}.

water molecules results in more uniform H-bonding. However, the narrowing may also be attributed to differences in vibrational relaxation times for water molecules H-bonding to other water molecules versus those H-bonding to glycerol. Homogeneous broadening increases peak width as the relaxation time decreases. Puzenko et al.[14] and Hayashi et al.[13] have shown that vibrational relaxation times of glycerol/water mixtures are influenced by concentration; increased water content leads to shorter vibrational relaxation times. Therefore, the narrowing in the HOH bend mode exhibited in Figure 12 may be an effect of slower water vibrational relaxation at high x_{glyc}. These results, coupled with the A1/A2 analysis, suggest that glycerol mimics the H-bonding that would form in ice by interacting with water molecules in more linear H-bonds.

IV. Conclusion

The average H-bonding patterns of water with increasing glycerol concentration indicate that, in mixtures with high water

content ($x_{glyc} < 0.15$), the average number of H-bonds/water from first hydration shell interactions grows at the expense of bulk water interactions (Figure 3). After the bulk water pool is depleted around $x_{glyc}(0.15)$, H-bonding in the first hydration shell becomes disrupted as glycerol molecules compensate for the lack of sufficient water molecules for solvation. The total average number of H-bonds/water decreases (Figure 3) and glycerol−glycerol interactions overtake glycerol−water interactions as the predominant H-bonding interaction in the solvation shell at $x_{glyc}(\sim 0.22)$ (Figure 4). By $x_{glyc}(0.27)$, the H-bonds between water molecules in the first hydration shell have been disrupted to such an extent that the percolation nature of the H-bond network is disturbed.

With depletion of the bulk water pool, the nature of first hydration shell water H-bonds also changes. As glycerol concentration increases through $x_{glyc}(0.27)$, the average number of H-bonds/first hydration shell water surrounding polar groups of glycerol increases relative to the number surrounding nonpolar groups (Figure 5). This result suggests that as glycerol concentration increases, water molecules in the first hydration shell become more likely to be associated with the glycerol OH groups than the alkyl backbone. This association is supported by trends seen in the IR spectra of the glycerol CH stretch region (Figures 6 and 7), which indicate that the nature of the C−H···O acceptor changes from $0 < x_{glyc} < 0.6$. Water, a stronger H-bond acceptor, becomes less available to H-bond with the alkyl backbone as glycerol concentration increases. At intermediate glycerol concentrations, the weaker glycerol OH groups may provide H-bond interactions with the alkyl backbone, while at high glycerol concentrations, clustering of alkyl groups may limit H-bond interactions.

Finally, it was shown that glycerol−water H-bonds become progressively more linear as glycerol concentration increases (Figure 8). With linearization of the glycerol−water H-bond, the strength of the interaction increases, and thus, the IR frequency of the associated OH stretch and HOH bend should decrease and increase, respectively. In fact, increased glycerol concentration causes a shift of the OH stretch mode to lower frequency (Figure 9, 295 K spectra) and a shift of the HOH bend mode to higher frequency (Figures 10 and 11). The information from the HOH bend mode is particularly useful since this mode represents contributions solely from water molecules. Narrowing of the HOH bend band with glycerol concentration (Figure 12) indicates possible reductions in homogeneous or inhomogeneous broadening that are associated with a reduction in H-bond angle distribution and an increase in vibrational relaxation time, respectively.

These results lend support to the conclusion that the combined affect of bulk water depletion, increase in alkyl backbone interactions, and H-bond linearization contributes to the cryoprotective properties of higher concentration glycerol/water mixtures. Interestingly, low temperature spectra of glycerol/water mixtures show that the peak frequency of the OH stretch is similar regardless of whether water crystallizes (Figure 9). When bulk water is present, as is the case in lower concentration mixtures, this water is able to freeze at low temperature and the resultant shift in IR frequency is observed. In the higher concentration mixtures where bulk water is depleted, freezing is not observed. However, linearization of H-bonds in the mixture still contributes to a frequency shift. The similar end peak position lends support to the notion that higher concentration glycerol/water mixtures mimic the H-bonding present in ice.

Increase in the distribution of linear glycerol−water H-bonds in higher glycerol concentration mixtures may also play a role in protein stabilization through preferential hydration. Our results support earlier experimental evidence that glycerol interacts favorably with water to strengthen the H-bond network of the solvent.[40] As glycerol concentration is increased, the chemical potential of the protein increases. To compensate for the change in chemical potential, solvent molecules at the surface of the protein must rearrange, either through altering glycerol/water H-bonding structure or through exclusion of glycerol molecules in the protein vicinity.[41−44] Therefore, protein unfolding, which exposes more surface area and hydrophobic groups, becomes even more thermodynamically unfavorable than unfolding in pure water, and the protein structure is stabilized.

Acknowledgment. This project was supported by the National Research Initiative of the USDA Cooperative State Research, Education and Extension Service, Grant 2005-35503-16151. Support from the NIH PO1 GM48130 for K.A.S. is greatly acknowledged. N.V.N. was supported by NIH F31 NS053399-02.

References and Notes

(1) Izawa, S.; Sato, M.; Yokoigawa, K.; Inoue, Y. *Appl. Microbiol. Biotechnol.* **2004**, *66*, 108−114.
(2) Izumi, Y.; Sonoda, S.; Yoshida, H.; Danks, H. V.; Tsumuki, H. *J. Insect Physiol.* **2006**, *52*, 215−220.
(3) Layne, J. R. *J. Exp. Zool.* **1999**, *283*, 221−225.
(4) Lewis, J. M.; Ewart, K. V.; Driedzic, W. R. *Physiol. Biochem. Zool.* **2004**, *77*, 415−422.
(5) Storey, K. B. *Comp. Biochem. Physiol.* **1997**, *117A*, 319−326.
(6) Davis-Searles, P. R.; Saunders, A. J.; Erie, D. A.; Winzor, D. J.; Pielak, G. J. *Annu. Rev. Biophys. Biomol. Struct.* **2001**, *30*, 271−306.
(7) Sousa, R. *Acta Crystallogr.* **1995**, *D51*, 271−277.
(8) Callam, C. S.; Singer, S. J.; Lowary, T. L.; Hadad, C. M. *J. Am. Chem. Soc.* **2001**, *123*, 11743−11754.
(9) Chelli, R.; Procacci, P.; Cardini, G.; Califano, S. *Phys. Chem. Chem. Phys.* **1999**, *1*, 879−885.
(10) Marcus, Y. *Phys. Chem. Chem. Phys.* **2000**, *2*, 4891−4896.
(11) Parsons, M. T.; Westh, P.; Davies, J. V.; Trandum, C.; To, E. C. H.; Chiang, W. M.; Yee, E. G. M.; Koga, Y. *J. Solution Chem.* **2001**, *30*, 1007−1028.
(12) To, E. C. H.; Davies, J. V.; Tucker, M.; Westh, P.; Trandum, C.; Suh, K. S. H.; Koga, Y. *J. Solution Chem.* **1999**, *28*, 1137−1157.
(13) Hayashi, Y.; Puzenko, A.; Balin, I.; Ryabov, Y. E.; Feldman, Y. *J. Phys. Chem. B* **2005**, *109*, 9174−9177.
(14) Puzenko, A.; Hayashi, Y.; Ryabov, Y. E.; Balin, I.; Feldman, Y.; Kaatze, U.; Behrends, R. *J. Phys. Chem. B* **2005**, *109*, 6031−6035.
(15) Doess, A.; Paluch, M.; Sillescu, H.; Hinze, G. *Phys. Rev. Lett.* **2002**, *88*, 095701.
(16) Fabri, D.; Williams, M. A. K.; Halstead, T. K. *Carbohydr. Res.* **2005**, *340*, 889−905.
(17) Mizuno, K.; Miyashita, Y.; Shindo, Y.; Ogawa, H. *J. Phys. Chem.* **1995**, *99*, 3225−3228.
(18) Vanderkooi, J. M.; Dashnau, J. L.; Zelent, B. *Biochim. Biophys. Acta* **2005**, *1749*, 214−233.
(19) Zelent, B.; Nucci, N. V.; Vanderkooi, J. M. *J. Phys. Chem. A* **2004**, *108*, 11141−11150.
(20) Mendelovici, E.; Frost, R. L.; Kloprogge, T. *J. Raman Spectrosc.* **2000**, *31*, 1121−1126.
(21) Gallagher, K. R.; Sharp, K. A. *J. Am. Chem. Soc.* **2003**, *125*, 9853−9860.
(22) Madan, B.; Sharp, K. A. *J. Phys. Chem.* **1996**, *100*, 7713−7721.
(23) Madan, B.; Sharp, K. A. *Biophys. Chem.* **1999**, *78*, 33−41.
(24) Sharp, K. A.; Madan, B. *J. Phys. Chem. B* **1997**, *101*, 4343−4348.
(25) Sharp, K. A.; Madan, B.; Manas, E.; Vanderkooi, J. M. *J. Chem. Phys.* **2001**, *114*, 1791−1796.
(26) Brooks, B. R.; Bruccolcri, R. E.; Olafson, B. D.; States, D. J.; Swaminathan, S.; Karplus, M. *J. Comput. Chem.* **1983**, *4*, 187−217.
(27) Reiling, S.; Schlenkrich, M.; Brickmann, J. *J. Comput. Chem.* **1996**, *17*, 450−468.
(28) Jorgensen, W. L.; Chandrasekhar, J.; Madura, J. D.; Impey, R. W.; Klein, M. L. *J. Chem. Phys.* **1983**, *79*, 926−935.
(29) Flick, E. W. *Industrial Solvents Handbook*, 5th ed.; Noyes Data Corporation/Noyes Publications: 1998.
(30) Ryckaert, J. P.; Ciccotti, G.; Berendsen, H. J. C. *J. Comput. Phys.* **1977**, *23*, 327−341.
(31) Gallagher, K. R.; Sharp, K. A. *Biophys. Chem.* **2003**, *105*, 195−209.

(32) Bastiansen, O. *Acta Chem. Scand.* **1949**, *3*, 415−421.
(33) Oleinikova, A.; Brovchenko, I.; Smolin, N.; Krukau, A.; Geiger, A.; Winter, R. *Phys. Rev. Lett.* **2005**, *95*, 247802.
(34) Sarkar, S.; Joarder, R. N. *Phys. Lett. A* **1996**, *222*, 195−198.
(35) Gu, Y.; Kar, T.; Scheiner, S. *J. Am. Chem. Soc.* **1999**, *121*, 9411−9422.
(36) Scheiner, S.; Kar, T. *J. Phys. Chem. A* **2002**, *106*, 1784−1789.
(37) Freda, M.; Onori, G.; Santucci, A. *J. Phys. Chem. B* **2001**, 105, 12714−12718.
(38) Yang, C.; Sharp, K. A. *Proteins: Struct., Funct., Bioinf.* **2005**, *59*, 266−274.
(39) Falk, M. *Spectrochim. Acta* **1984**, *40A*, 43−48.
(40) McDuffie, J.; G. E., Quinn, R. G.; Litovitz, T. A. *J. Chem. Phys.* **1962**, *37*, 239−242.
(41) Betting, H.; Haeckel, M.; Hinz, H.-J.; Stockhausen, M. *Phys. Chem. Chem. Phys.* **2001**, *3*, 1688−1692.
(42) Brandts, J. F.; Hunt, L. *J. Am. Chem. Soc.* **1967**, *89*, 4826−4838.
(43) Gekko, K.; Timasheff, S. N. *Biochemistry* **1981**, *20*, 4667−4676.
(44) Gerlsma, S. Y. *J. Biol. Chem.* **1968**, *243*, 957−961.